Supporting Information Appendix

For

Biomineralization by particle attachment in early animals

Pupa U. P. A. Gilbert[a,b,#,*], Susannah M. Porter[c], Chang-Yu Sun[a], Shuhai Xiao[d], Brandt M. Gibson[e], Noa Shenkar[f,g], Andrew H. Knoll[h*]

a. Department of Physics, University of Wisconsin, Madison, WI 53706.

b. Departments of Chemistry, Materials Science and Engineering, and Geoscience, University of Wisconsin, Madison, WI 53706, USA.

c. Department of Earth Science, University of California at Santa Barbara, Santa Barbara, CA 93106.

d. Department of Geosciences, Virginia Tech, Blacksburg, VA 24061, USA.

e. Department of Earth and Environmental Sciences, Vanderbilt University, Nashville, TN 37235, USA.

f. School of Zoology, George S. Wise Faculty of Life Science, Tel-Aviv University, Tel Aviv, 69978 Israel.

g. The Steinhardt Museum of Natural History, National Research Center for Biodiversity Studies, Tel-Aviv University, Tel Aviv, 69978 Israel.

h. Department of Organismic and Evolutionary Biology, Harvard University, Cambridge, MA 20138, USA.

Previously publishing as Gelsomina De Stasio

* Corresponding authors: pupa@physics.wisc.edu, aknoll@oeb.harvard.edu.

www.pnas.org/cgi/doi/10.1073/pnas.1902273116

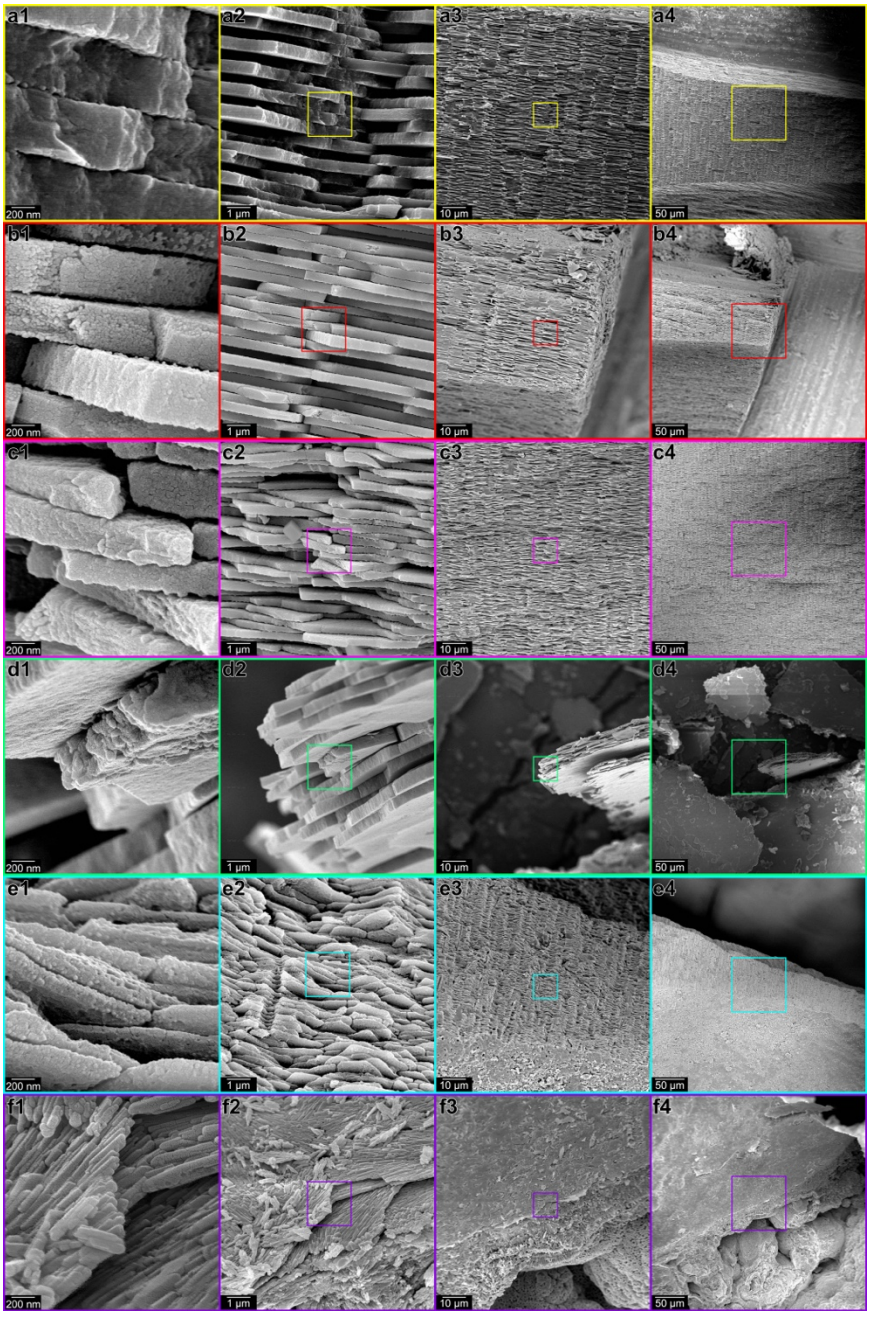

Figure S1. Decreasing magnification SEM images of the same areas in Fig. 2. Panels 1 are identical to those in Fig. 2, whereas panels 2, 3, 4 show images acquired progressively zooming-out while maintaining precisely the same location (co-centered and co-labeled in the main text and hereafter). In all panels 2-4 boxes indicate where the previous, higher-magnification image in panels 1-3 was acquired.
a1-4. Modern *Haliotis rufescens*, cryofractured.
b1-4. Modern *Haliotis rufescens*, cryofractured, bleached, etched.
c1-4. Modern *Nautilus pompilius*, cryofractured, bleached, etched.
d1-4. Miocene (~13 Ma) bivalve nacre from *Atrina harrisii*. This nacre is still aragonite (1).
e1-4. Cretaceous (~100 Ma) baculite cephalopod nacre, cryofractured, bleached, etched.
f1-4. Ordovician (~450 Ma) phosphatized nacre from the cephalopod *Isorthoceras sociale*.

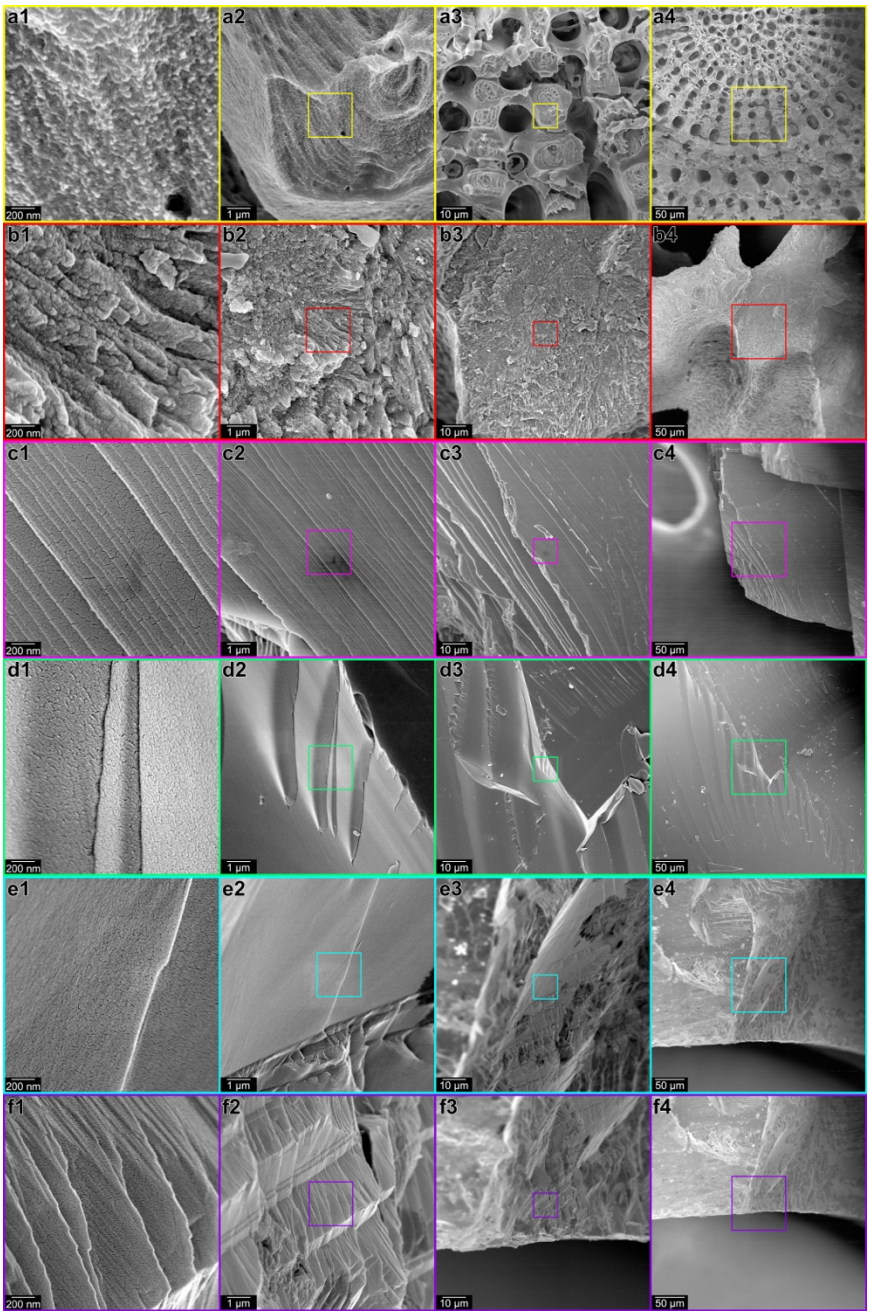

Figure S2. Decreasing magnification SEM images of the same areas in Fig. 3, co-centered and co-labeled, with boxes indicating where the previous image was acquired.
a1-4. Sea urchin spine, cryofractured, etched.
b1-4. Coral skeleton, cryofractured.
c1-4. Non biogenic calcite, cryofractured.
d1-4. Non-biogenic apatite.
e1-4. Non-biogenic aragonite, with typical featureless appearance.
f1-4. Non-biogenic aragonite, with rare feature-rich surface.

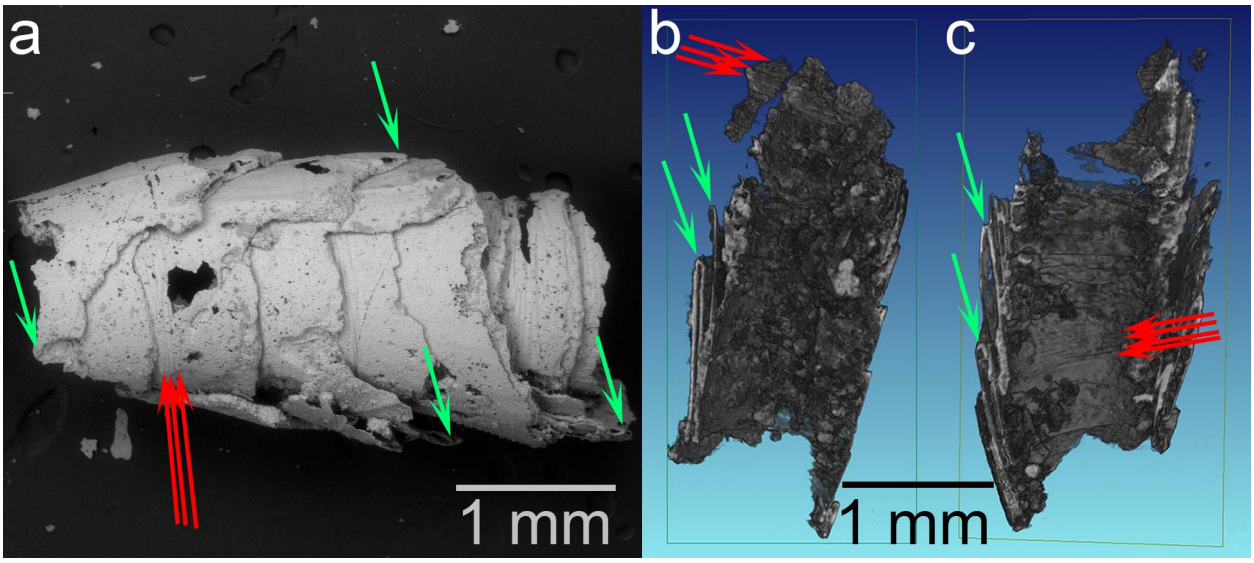

Figure S3. SEM image and X-ray micro-CT cut-off views of *Cloudina* specimen 111-2 (3) shown in Figure 4, acquired before it was fractured. a. SEM image showing nested funnels typical of *Cloudina*. Red arrows point at external annulations, green arrows at rounded edges of funnels.

See Cloudina.avi movie for animated X-ray micro-CT images of this sample.

b–c. X-ray micro-CT bisected views of longitudinal cross sections, showing double-walled funnels, with rounded edges (green arrows) and annulations on internal surface (red arrows). These low-resolution data already reveal some anatomical details not previously documented in *Cloudina*, which were confirmed in greater detail (Figures 4, S4 and S5). Five important observations include:

1. Each *Cloudina* funnel is double walled. The connection between the inner and outer walls, best visible in Figure S5c2,c3, suggests that the double-walled funnels are biological structures, not diagenetic or sample preparation artifacts resulting from partial dissolution of the middle portion of a single wall.
2. The double-walled funnels end with rounded edges at the wider and narrower ends of each funnel (green arrows in a, b, c).
3. Annulations (red arrows) appear on the outer (a) and inner (b, c) surfaces of each funnel, confirming observations made by Cai et al. (2). Based on their appearance and position, we speculate that the annulations may have served to imbricate and lock the funnels in position.
4. *Cloudina* funnel walls consist of irregularly shaped nanoparticles, as best seen on fractured cross section of the walls (Figures 4 and S4).
5. Smooth thin layers line the inside and outside of each funnel wall (Figures S4h,i and S5a2,b2,c2).

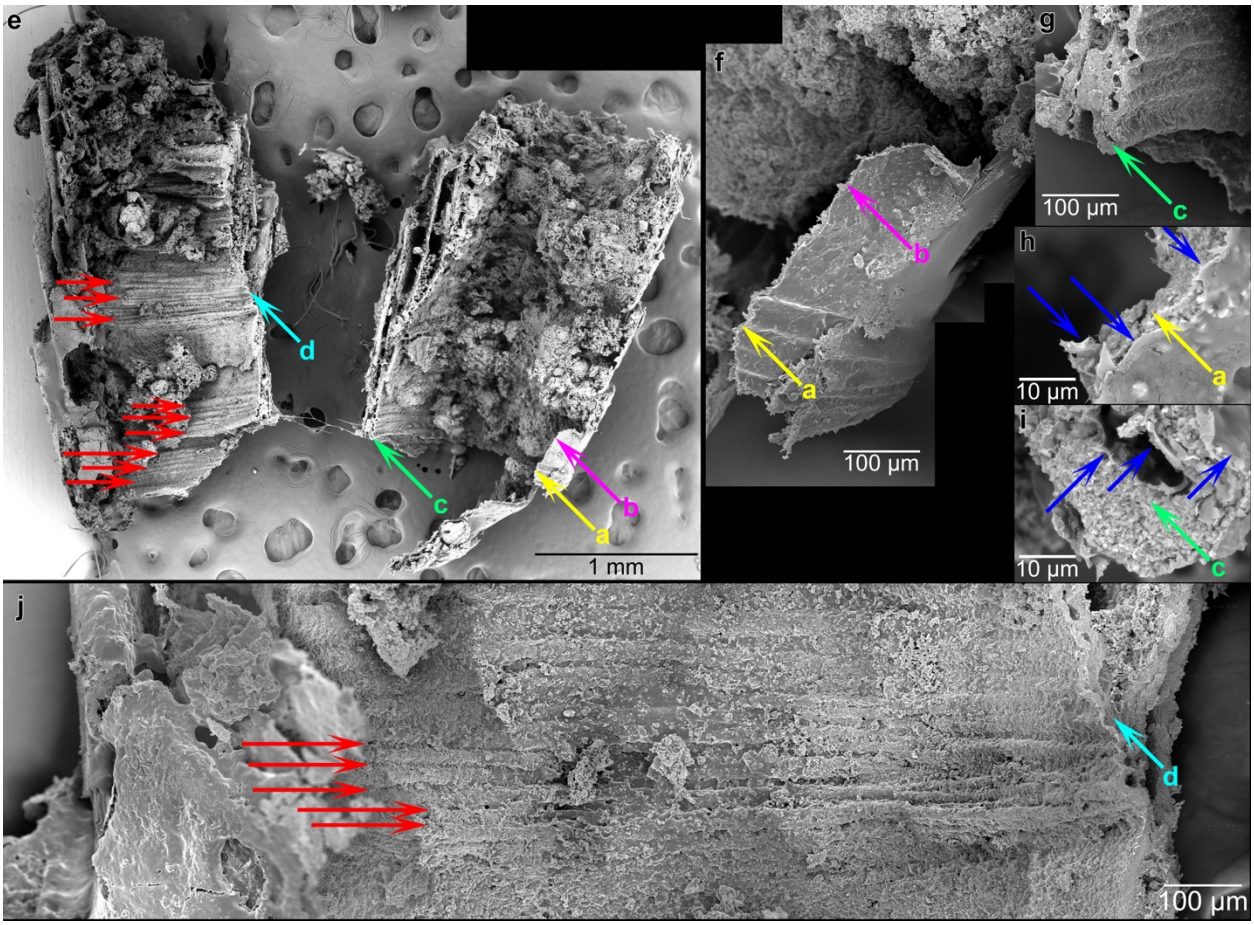

Figure S4. Low magnification SEM images of the same *Cloudina* specimen in Figure S3, after it was fractured. The areas imaged in Figure 4 and S5 are correspondingly labeled a-d. The images in panels e, h, and i were acquired in backscattered electron (BSE) mode, all others in secondary electron mode. Blue arrows in panels h and i indicate some of the smooth layers observed inside and outside funnel walls. Since these layers appear bright in BSE, they cannot be organic at present. If they were organic when the animal deposited them, they became mineralized during diagenesis. Red arrows in panels e and j point at annulations, which extend across the entire funnel width but not along the entire funnel length (2). This is imaged at higher magnification in j, showing the inside of a *Cloudina* funnel, but similar annulations are observed in every *Cloudina* funnel on the inner (e) and outer (f) surfaces. As mentioned in Figure S3, we suggest that the annulations may have served to imbricate and lock the funnels in place.

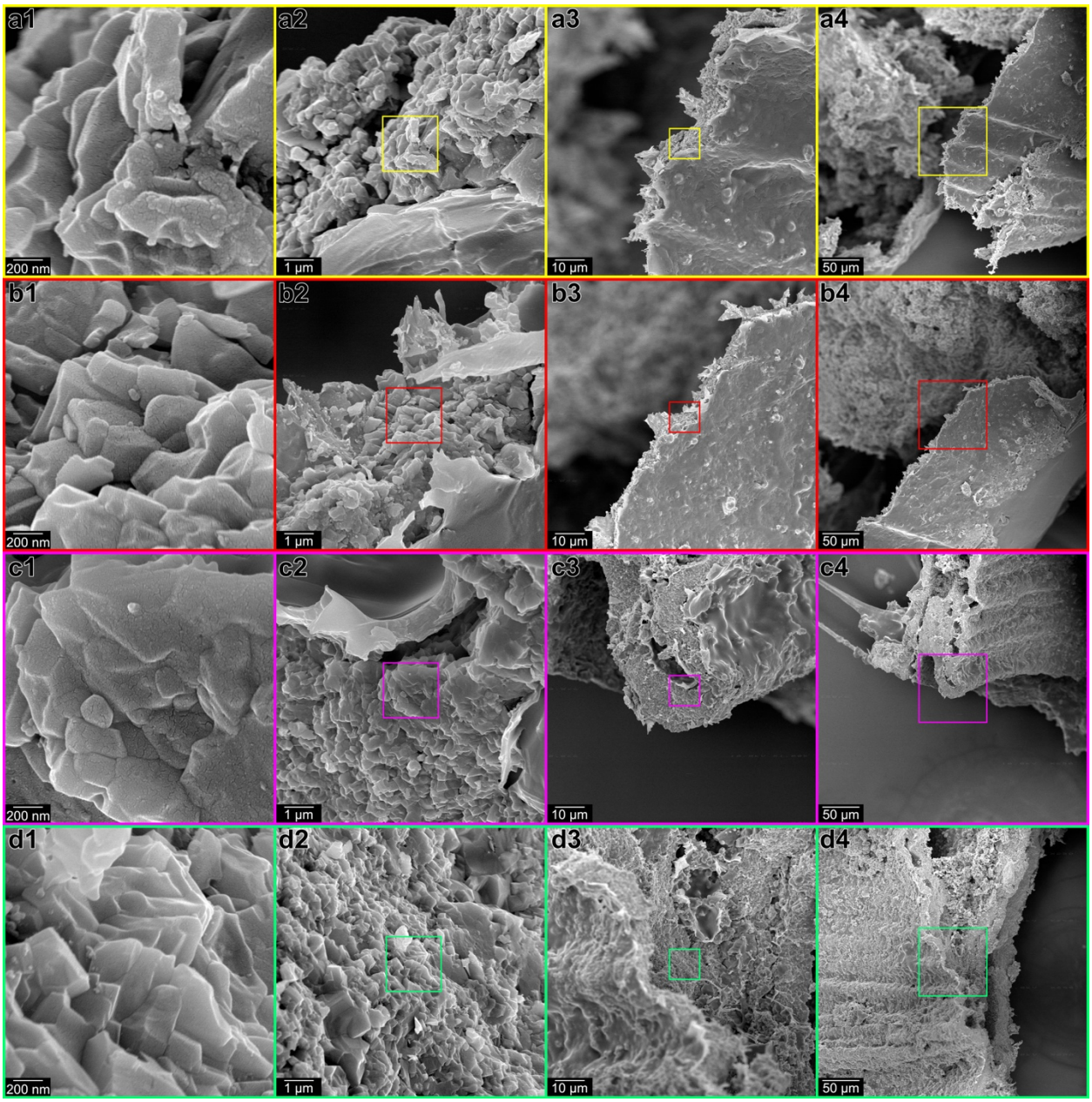

Figure S5. Lower-magnification SEM images of *Cloudina* as in Figure 4, co-centered and co-labeled. Notice several new observations, not previously reported: panels a2-a3 and b2-b3 and c2-c3 show smooth layers inside and outside of fractured *Cloudina* funnel walls. These layers are also imaged and discussed in Figure S4. Panels c2-c4 and d3-d4 show that each *Cloudina* funnel is double-walled, and the two walls are joined to form a rounded folding at the top and bottom edges of each funnel (see for example c3). Panels d3-d4 show that *Cloudina* funnels are annulated on both the inner and outer layers (2). These crenulations are also shown and discussed in Figure S4.

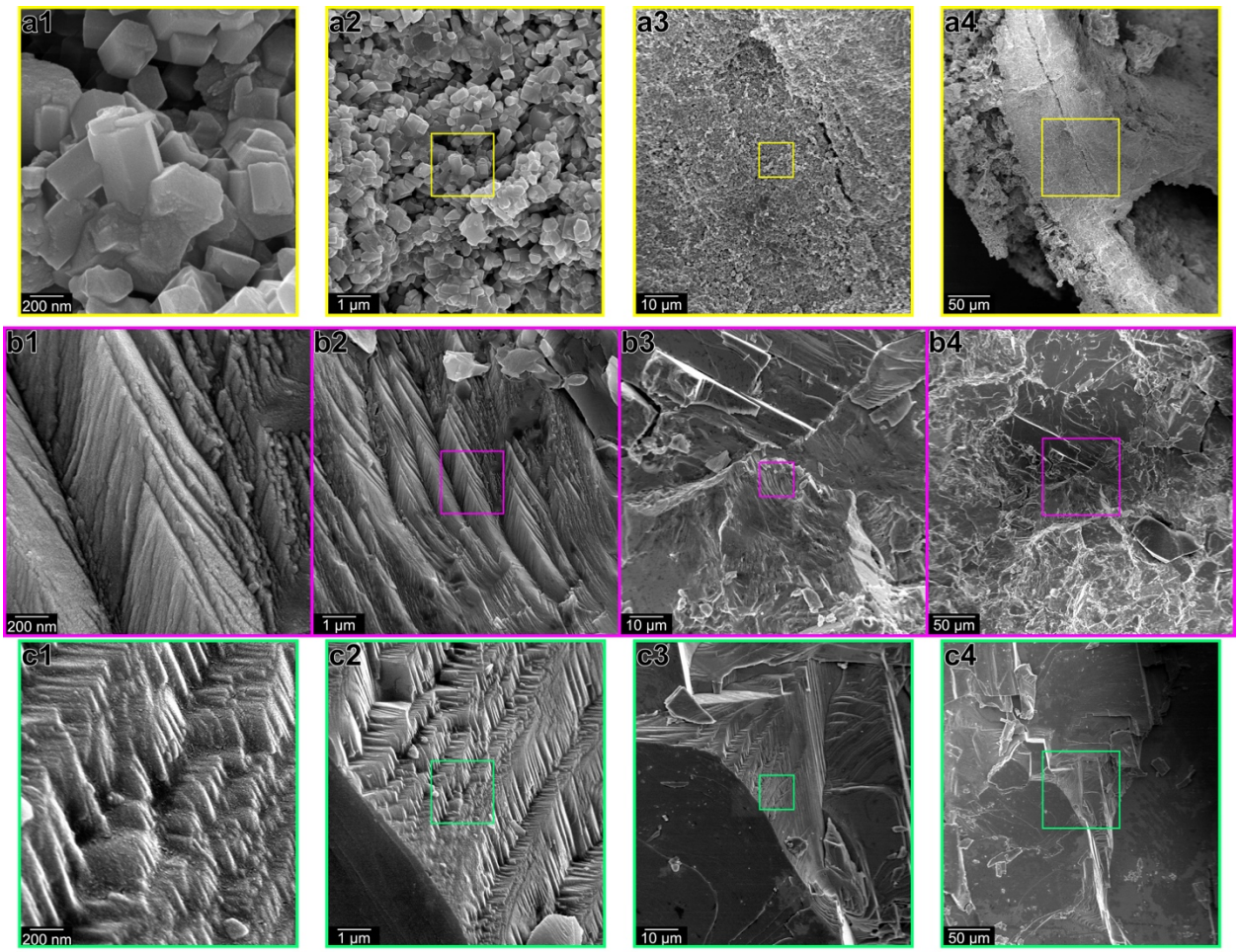

Figure S6. a1-4: Phosphatized *Cloudina* specimen 102-1-1 from China, showing a double-walled funnel cross-section, fractured by us, that exhibits nanoscale hexagonal prisms, the typical crystal habit of euhedral apatite crystals. Interestingly, this region of the *Cloudina* funnel wall did not re-crystallize into a large single crystal as the one in a1-4 but as nanocrystals of a similar size to those in Figure 4, suggesting that dissolution and reprecipitation of apatite occurred one nanoparticle at a time. Before dissolution the nanoparticles may have been already phosphatized, or may have been carbonates. The only directly observable evidence is that after reprecipitation they are hexagonal apatite prisms, which resist maceration in acetic acid. b1-4: Cryofractured re-crystallized *Cloudina* from Namibia, showing fracture ridges with acute angles, parallel to one another, suggesting a single crystalline sample. Acute angles suggest calcite. c1-4: Single-crystalline geologic calcite cryofractured in mortar and pestle, showing many ridges parallel to one another, with obtuse angles. Even though these angles are obtuse and those in *Cloudina* acute, both are consistent with calcite rhombohedra, which have obtuse and acute angles. We note that Pruss et al. recently argued that *Cloudina* had aragonitic shells. Since re-crystallization usually occurs in the direction of the most thermodynamically stable polymorph, our observation of calcite does not contradict Pruss *et al*. (3).

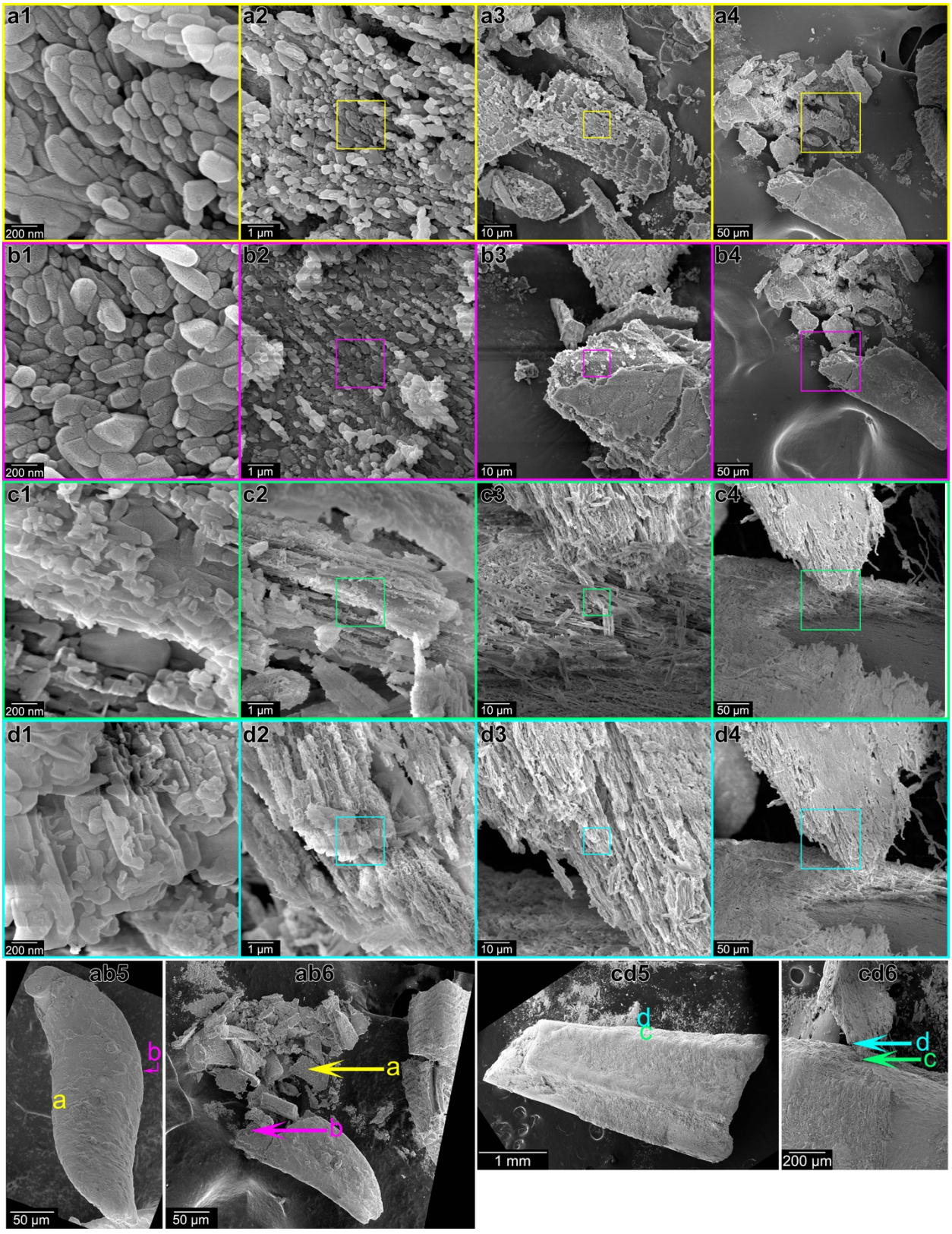
a1
200 nm
a2
1 µm
a3
10 µm
a4
50 µm
b1
200 nm
b2
1 µm
b3
10 µm
b4
50 µm
c1
200 nm
c2
1 µm
c3
10 µm
c4
50 µm
d1
200 nm
d2
1 µm
d3
10 µm
d4
50 µm
ab5
a
b
50 µm
ab6
a
b
50 µm
cd5
d
c
1 mm
cd6
d
c
200 µm

Figure S7. Decreasing magnification SEM images of the same regions in Figure 5, co-labelled and co-centered. These same fossils were also imaged before (ab5, cd5) and after fracturing (ab6, cd6). In all panels 2-4 boxes indicate where the previous, higher-magnification image was acquired. In panels ab5, ab6, cd5, cd6 the letters a, b, c, d refer to the approximate location of the unbroken sample where the correspondingly labeled images here and in Figures 5a,b,c,d were acquired. Mounting and tilt angles are not identical from one SEM to another, but the features are easily recognizable. The halkieriid sclerite in ab5 and ab6 rotated around its long axis when it was fractured, but all other specimens remained in this work approximately in the same orientation.
a1-a4. A sclerite of the halkieriid *Australohalkieria superstes* (4) with a phosphatized cast of the wall surrounded by an external mold (underneath the cast in a3). In a1-a3, the view is from the interior of the sclerite looking toward the outer surface.
b1-b4. A different region of the same halkieriid sclerite in a1-a4.
c1-c4. A hyolith with a phosphatized cast of the shell wall consisting of nanoscale filaments. The smooth surface of the internal mold can be seen to the right in b4 underneath the broken cast.
d1-d4. A different cross-section region of the same hyolith in c1-c4. A careful inspection reveals absolutely no euhedral crystals anywhere in these or any other images from these two samples. Plentiful euhedral crystals appear in the fossils of Figures S8 and S9.

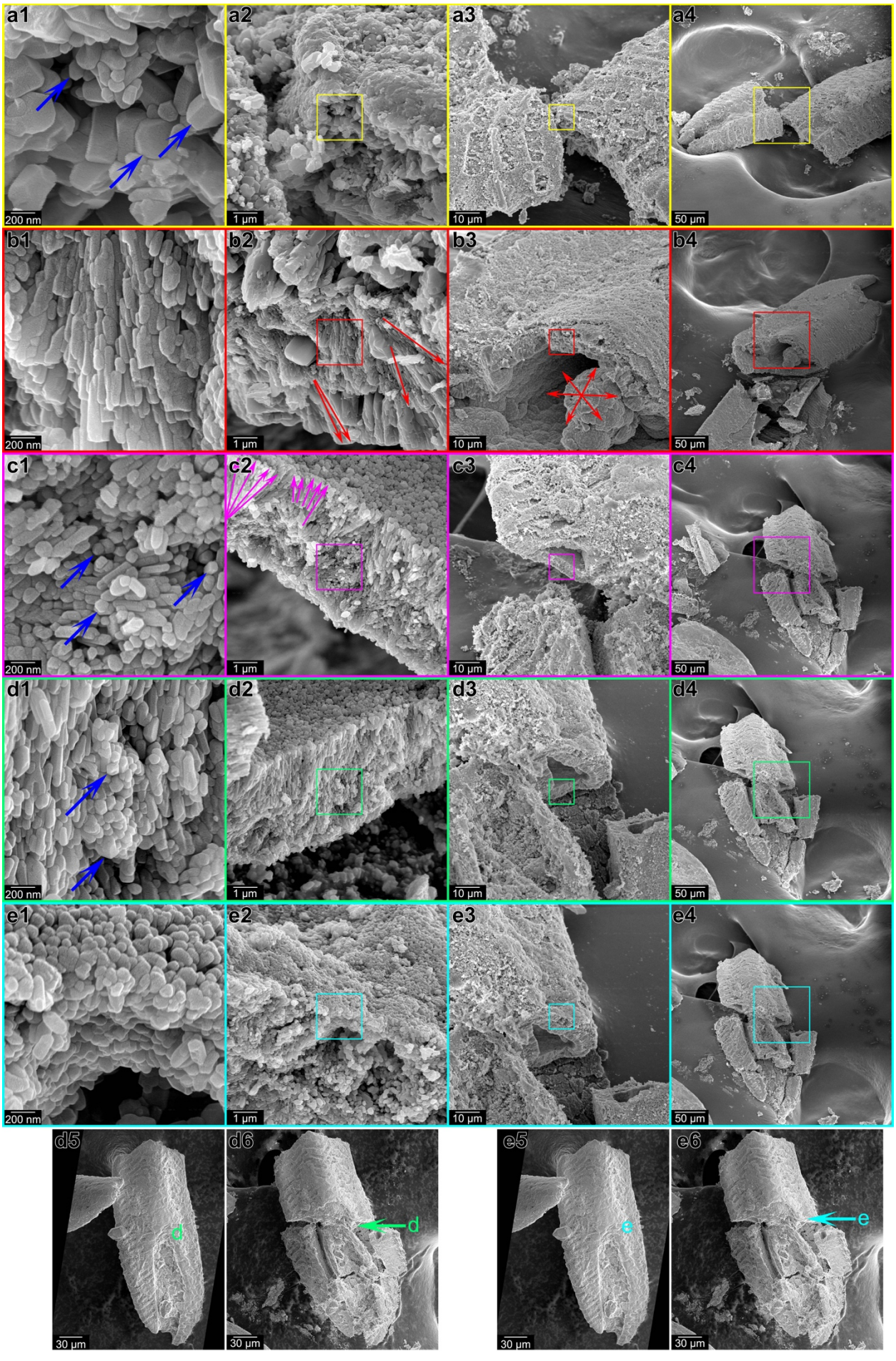
a1
200 nm
a2
1 μm
a3
10 μm
a4
50 μm
b1
200 nm
b2
1 μm
b3
10 μm
b4
50 μm
c1
200 nm
c2
1 μm
c3
10 μm
c4
50 μm
d1
200 nm
d2
1 μm
d3
10 μm
d4
50 μm
e1
200 nm
e2
1 μm
e3
10 μm
e4
50 μm
d5
d
30 μm
d6
d
30 μm
e5
e
30 μm
e6
e
30 μm

Figure S8. Decreasing magnification SEM images of a recrystallized *Australohalkieria superstes* sclerites. Again, boxes in panels 2-4 indicate where the previous, higher-magnification image was acquired.
a1-a4. Recrystallized sclerite wall.
b1-b4. Spherulitic internal mold. The spherulitic arrangement of acicular crystals is most evident in in b2 (red arrows indicate a few, but there are many more acicular crystals arranged radially).
c1-c4. Another spherulitic internal mold in a different halkieriid *Australohalkieria superstes* sclerite. The spherulitic acicular crystals are best shown in c2 (magenta arrows indicate a few, many more exist). Blue arrows in a1, c1, d1 d1 indicate euhedral, hexagonal crystals, typical of apatite.
d, e. The same phosphatized halkieriid sclerite in c, imaged in two different locations.
d1-d4. The internal mold of the *A. superstes* sclerite, also phosphatized, but exhibiting prism crystals seen from a side. Rarely in this image the crystalline prisms are seen in cross-section, but, where they are, they appear hexagonal (blue arrows in d1).
e1-e4. The thin outer layer of the same halkieriid sclerite in c and d. This outer layer exhibits rounded, globular nanoparticles and was previously proposed to be originally an organic outer layer, akin to the periostracum observed in modern mollusk shells (see Porter 2004b (5)). If one zooms-in on this figure and looks carefully for euhedral crystals, one finds them in a, b, c, d, and at the bottom of e, which is also an internal mold. In Figure S7, instead, even after zooming-in and looking carefully no euhedral crystals can be identified.
Panes d5,6 and e5,6 show the same halkieriid sclerite from *Australohalkieria superstes* in d1-4,e1-4, imaged at the SEM before (d5-e5) and after breaking with one SEM (d6-e6). The letters d, e in panels 5 and 6 refer to the approximate location of the unbroken sample where the correspondingly labeled images in 1-4 were acquired.

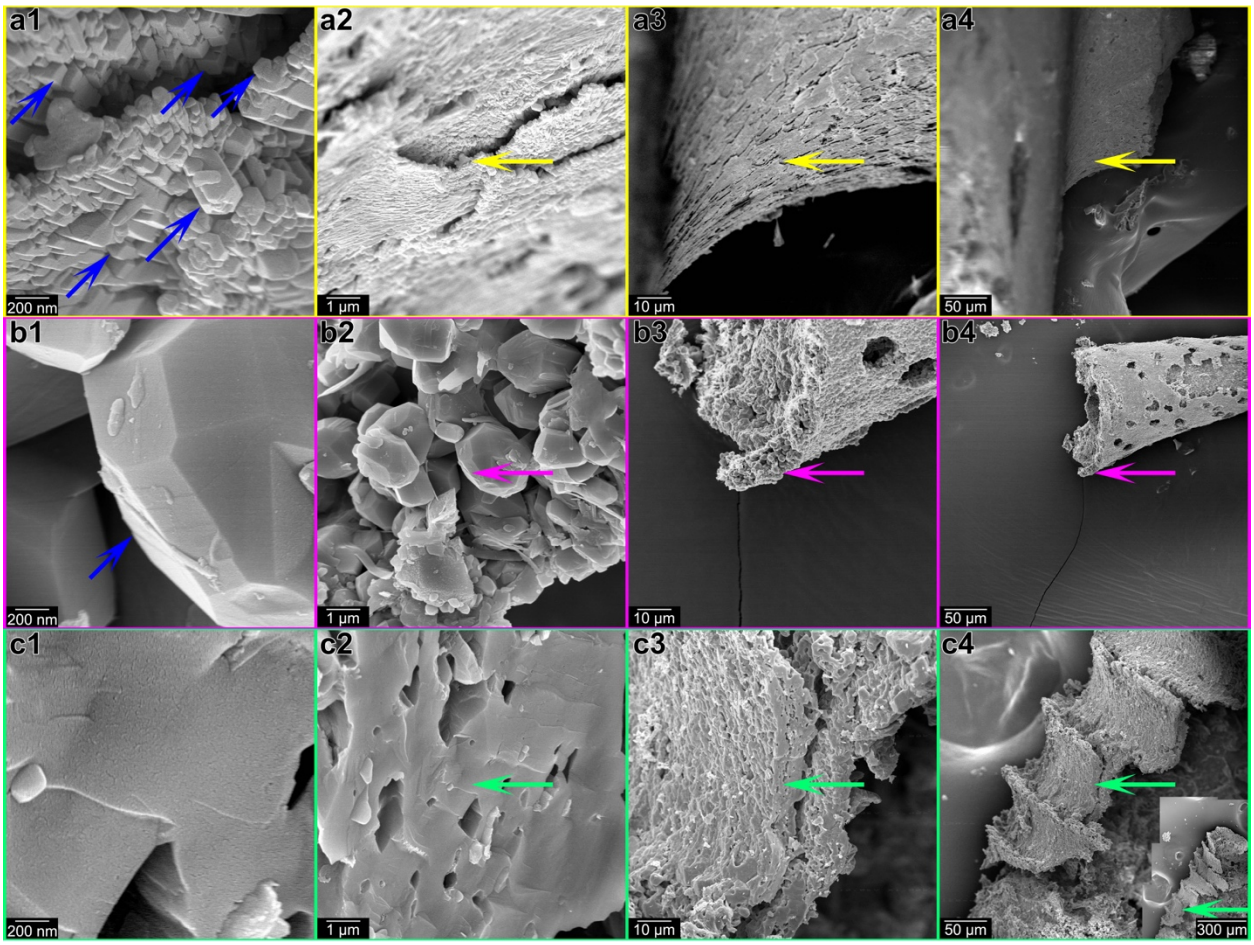

Figure S9. Decreasing magnification SEM images of recrystallized fossil nacre and other shelly fossils. As in other figures, horizontal arrows in panels 2-4 indicate the center of the image, where the previous, higher-magnification image was acquired, and blue arrows in a1 and b1 point at euhedral, hexagonal crystals, typical of apatite and calcite, respectively.

a1-a4. Recrystallized, phosphatized Upper Ordovician nacre from *Isorthoceras sociale*. Note that even after re-crystallization to nanoscale euhedral crystals, nacre remains layered. In fact, this sample was selected as it shows iridescence visible to the naked eye. Furthermore, the nanoscale euhedral crystals indicate that dissolution and re-precipitation occurred one nanoparticle at a time.

b1-b4. Pseudomorphic calcite crystals in the fractured wall of a sclerite from the early Cambrian chancelloriid *Archiasterella hirundo* (6) The crystals have a habit typical of calcite, but they were pseudomorphed by phosphate and as such did not dissolve during maceration in acetic acid.

c1-c4. Fractured cross-section of the Cambrian mollusk shell *Yochelcionella snorkorum* (7), showing a mono-block crystal, suggesting that dissolution and re-crystallization did not occur one nanoparticle at a time but in bulk amount at once. Inset in c4 shows a lower magnification SEM image of the same mollusk shell, and its many scalloped ridges typical of many bivalve shells.

SI References

1. Gilbert, PUPA et al. (2017) Nacre tablet thickness correlates with temperature in recent and fossil shells. *Earth Planet Sci Lett* 460:281-292.
2. Cai Y, Cortijo I, Schiffbauer JD, Hua H (2017) Taxonomy of the late Ediacaran index fossil *Cloudina* and a new similar taxon from South China. *Precambrian Res* 298:146-156.
3. Pruss SB, Blättler CL, Macdonald FA, Higgins JA (2018) Calcium isotope evidence that the earliest metazoan biomineralizers formed aragonite shells. *Geology* 46:763-766.
4. Porter SM (2004a) Halkieriids in Middle Cambrian phosphatic limestones from Australia. *J Paleontol* 78:574-590.
5. Porter SM (2004b) Halkieriids in Middle Cambrian phosphatic limestones from Australia. *J Paleontol* 78:574-590.
6. Porter SM (2008) Skeletal microstructure indicates chancelloriids and halkieriids are closely related. *Palaeontology* 51:865–879.
7. Vendrasco MJ, Porter SM, Kouchinsky A, Li G, Fernandez CZ (2010) New data on molluscs and their shell microstructures from the Middle Cambrian Gowers Formation, Australia. *Palaeontology* 53:97-135.

Video S1

Movie of *Cloudina*, showing spatial distribution of skeletal and non-skeletal minerals.